https://doi.org/10.5194/wes-2019-89
Preprint. Discussion started: 4 December 2019
© Author(s) 2019. CC BY 4.0 License.

eawe european academy of wind energy
Open Access WIND ENERGY SCIENCE DISCUSSIONS

Measuring dynamic wake characteristics with nacelle mounted LiDAR systems

Inga Reinwardt[1], Levin Schilling[1], Peter Dalhoff[1], Dirk Steudel[2], and Michael Breuer[3]

[1]Dep. Mechanical Engineering & Production, HAW Hamburg, Berliner Tor 21, D-20099 Hamburg, Germany
[2]Dep. Turbine Load Calculation, Nordex Energy GmbH, Langenhorner Chaussee 600, D-22419 Hamburg, Germany
[3]Dep. of Fluid Mechanics, Helmut-Schmidt University Hamburg, Holstenhofweg 85, D-22043 Hamburg, Germany

Correspondence: Inga Reinwardt (inga.reinwardt@haw-hamburg.de)

Abstract. Light Detection And Ranging (LiDAR) systems have gained a great importance in today's wake characteristic measurements. The aim of this measurement campaign is to track the wake meandering and in a further step to validate the wind speed deficit in the meandering frame of reference (MFR) and in the fixed frame of reference using nacelle mounted LiDAR measurements. The measurement campaign has been prepared in detail by preliminary simulations mimicking the LiDAR behavior and corresponding wind field simulations. Additionally, a comparison between the modelled wake degradation in the MFR and the measured one could be conducted. The simulations were done with two different versions of the Dynamic Wake Meandering (DWM) model. These versions differ only in the description of the quasi-steady wake deficit. Based on the findings from the LiDAR measurements the formulation of the quasi-steady wake deficit in the DWM model has been adjusted, so that the recalibrated model coincides very well with the measurements.

1 Introduction

Wake calculation of neighbouring wind turbines is a key aspect of every wind farm development. The aim is to estimate both, energy yield of the whole windfarm and loads on single turbines, as accurately as possible. One of the main models for calculating the wake-induced turbulence in a wind farm is the so-called Frandsen model (see, for example, Frandsen (2007)). Previous measurement campaigns have shown that this model delivers conservative results for small turbine distances (Reinwardt et al. (2018) and Gerke et al. (2018)). This is particularly important for onshore wind farms in densely populated areas, where a high energy output per utilized area is crucial. In such cases, the usage of a more accurate description of the physical behaviour of the wake, as defined in the DWM model, seems appropriate. The DWM model is based on the assumption that the wake behaves as a passive tracer, which means, the wake itself is deflected in vertical and horizontal direction (Larsen et al., 2008b). The combination of this deflection and the shape of the wind speed deficit leads to an increased turbulence at a fixed position downstream. This plays an eminent role for the loads of a turbine located downstream of another turbine (Larsen et al., 2013). Therefore, a precise description of the meandering itself and the wind speed deficit in the meandering frame of reference (MFR) as well as a detailed validation of the wind speed deficit definition is fundamental.

https://doi.org/10.5194/wes-2019-89
Preprint. Discussion started: 4 December 2019
© Author(s) 2019. CC BY 4.0 License.

eawe european academy of wind energy
Open Access WIND ENERGY SCIENCE DISCUSSIONS

LiDAR systems are highly suitable for wake validation purposes. Especially, the so-called scanning LiDAR systems, which are capable of measuring a two-dimensional wind field, offer great potential for detailed wake analysis. With a scanning LiDAR device it is possible to detect the wake meandering as well as the shape of the wind speed deficit in the MFR. That is the reason why such a device is used in the measurement campaign outlined here. Several different measurement campaigns with ground based and nacelle mounted LiDAR systems have already been carried out in the last years, some of them even with the purpose of tracking wake meandering and validation of wake models.

In Bingöl et al. (2010) the horizontal meandering has been examined with a nacelle installed continuous wave (CW) LiDAR. The campaign confirms the passive tracer assumption, which is essential for the definition of the meandering in the DWM model. Furthermore, the wind speed deficit in the MFR has been investigated for some distances. Due to the fact that the CW LiDAR can not measure simultaneously in different downstream distances, the beam has been focused successively to different downstream distances. In Trujillo et al. (2011) the analysis has been extended to a two-dimensional scan. The measured wind speed deficit in the MFR has been compared to the Ainslie wake model (see Ainslie (1988)), which constitutes the basis of the deficit's definition in the DWM model.

Additionally, in Machefaux et al. (2013), a comparison of measured lateral wake meandering based on pulsed scanning LiDAR measurements has been presented. Special attention is paid to the advection velocity of the wake, which is estimated with measured and low-pass filtered wind directions at the metmast (based on the assumptions of the DWM model) and the wake displacement at certain downstream distances. The analysis shows that the advection velocity calculated by the N.O. Jensen model is in relatively good agreement. Finally, the study compares the measured expansion of the wake in the fixed frame of reference (FFR) to CFD simulations and simple analytical engineering models. The wake expansion calculated by simple analytical engineering models is well in line with LiDAR measurements and CFD simulations, but also depicts potential for further improvements, which is why a new empirical model for single-wake expansion is proposed in Machefaux et al. (2015). In Machefaux et al. (2016) a measurement campaign is presented, which involves three nacelle mounted CW scanning LiDAR devices. The investigation includes a spectral analysis of the wake meandering, a comparison of the measurements to the assumptions in the DWM model as well as a comparison of the wind speed deficit profile in a merged wake situation to CFD simulations.

It should be noted that the references listed here are only the most essential, on which the present measurement campaign builds up. Several campaigns including either LiDAR systems or meandering observations as well as wake model validations have been conducted in the past. The outlined analysis transfers some of the procedures of tracking the wake meandering to measurement results from an onshore wind farm with small turbine distances. Particular focus is put on the investigation of the wind speed deficit's shape in the MFR and the degradation of the wind speed deficit in downstream direction. The latter can be captured very well with the used nacelle mounted pulsed scanning LiDAR systems due to the fact that it measures simultaneously in different downstream distances. Thus, a detailed comparison of the predicted degradation of the wind speed deficit between the DWM model and the measurement results is possible.

https://doi.org/10.5194/wes-2019-89
Preprint. Discussion started: 4 December 2019
© Author(s) 2019. CC BY 4.0 License.

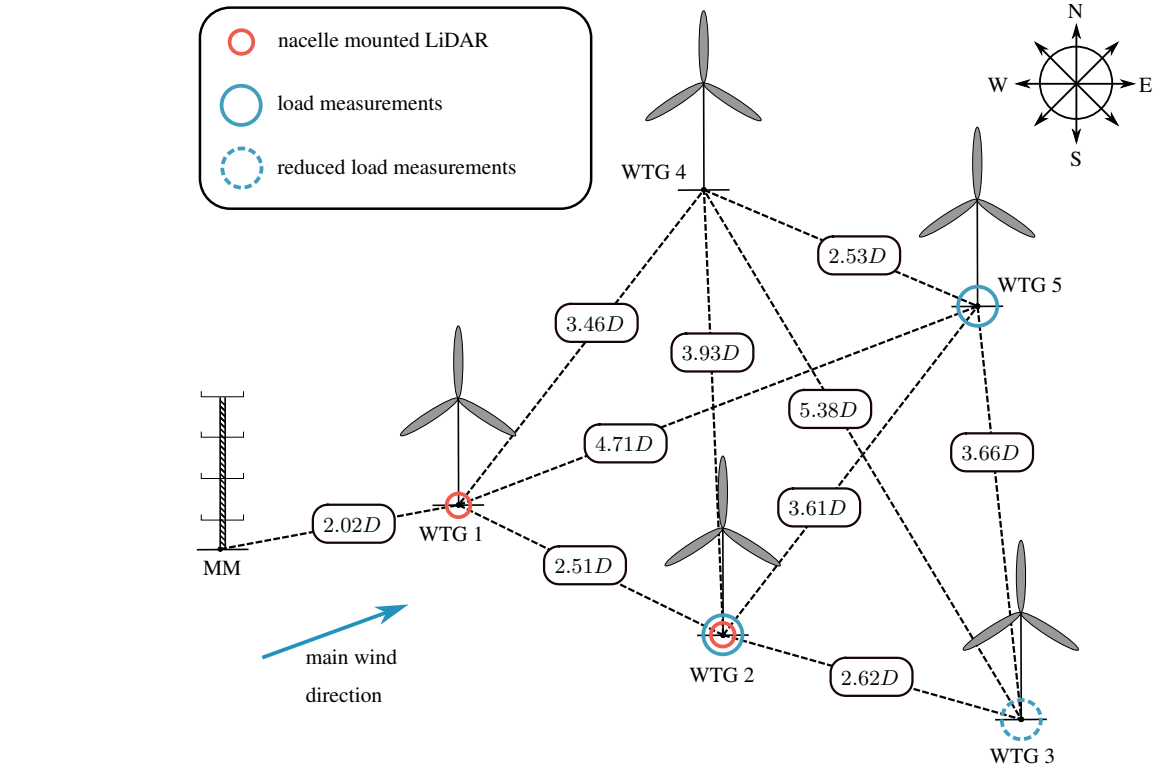

Figure 1. Wind farm layout with measurement equipment.

In the following, the investigated wind farm and the installed measurement equipment are described in detail. Afterwards, an explanation of the data processing and filtering of the measurement results is given. Furthermore, a description of the theoretical backround and a hands-on implementation of the DWM model is introduced. Based on the outlined measurement results, a recalibration of the defined degradation of the wind speed deficit in the DWM model is proposed. A summary of the measurement results and a comparison to the original DWM model as well as the recalibrated version is presented in the last sections.

2 Wind farm

The investigated onshore wind farm located in the Southeast of Hamburg (Germany) consists of five Nordex turbines (1x N117 3 MW and 4x N117 2.4 MW) with small turbine distances and a metmast, which is situated two rotor diameters ($D = 117$ m) ahead of the wind farm in main wind direction (west-southwest). There are no other turbines in the immediate vicinity and the terrain is mostly flat. Only in further distances (more than 1 km) the terrain is slightly hilly (approx. 40 m). Two turbine nacelles are equipped with a pulsed scanning LiDAR system (Galion G4000). Furthermore, three turbines are equipped with load measurements. The wind farm layout with all previously mentioned measurement devices is shown in Figure 1. The

https://doi.org/10.5194/wes-2019-89
Preprint. Discussion started: 4 December 2019
© Author(s) 2019. CC BY 4.0 License.

eawe european academy of wind energy
Open Access WIND ENERGY SCIENCE DISCUSSIONS

Table 1. Considered wind direction sectors per wake generating turbine in the measurement campaign. Wind direction sectors without free inflow of the metmast and the turbine as well as measurements in the induction zone of another turbine are omitted.

	lower limit [°]	upper limit [°]
WTG 1	160	190
	320	350
WTG 2	150	160
	240	250

LiDAR system of WTG 1 is installed inside the nacelle and measures through a hole in the rear wall. The second LiDAR system is installed on top of the nacelle of WTG 2, also facing backwards. Nacelle mounted GPS systems help tracking the nacelle's precise position as well as yaw movements.

3 Data filtering and processing

The measured LiDAR data are filtered and sorted in accordance with ambient wind speed, ambient turbulence intensity, wind shear, atmospheric stability, and wind direction. The ambient conditions are determined by the metmast, so that only measurement results with free inflow at the metmast are considered. Additionally, results without free inflow of the wake generating turbine as well as LiDAR measurements in the induction zone of another turbine are rejected. This leads to the remaining wind direction sectors listed in Table 1. The remaining sectors are relatively small, especially for the LiDAR on WTG 2, which reduces the amount of usable measurement data drastically. Atmospheric stability is determined by the gradient Richardson number, which is calculated with temperature and wind speed measurements at two different heights. A negative Richardson number implies unstable and a positive Richardson number stable atmospheric stratification. Only situations with normal power production of the wake generating turbine are considered. The turbine operation mode is identified through the turbine's Supervisory Control and Data Acquisition (SCADA) system. The LiDAR data are moreover filtered by the power intensity of the measurement results, which is closely related to the signal-to-noise ratio (SNR) of the measurements. Results with an intensity lower than 1.01 have been discarded. The range gate length of the LiDAR system is 30 m. The measurement time increases with the number of range gates due the fact that the internal data processing time increases. Thus, to decrease the measurement time, the number of range gates has been limited, so that the farthest scan point is 750 m downstream. Additionally, the scanning time of each horizontal line scan is verified by the timestamp of each scan to ensure that the meandering can really be captured.

LiDAR systems measure the line of sight (LOS) velocity. The wind speed in downstream direction is then calculated from the LiDAR's LOS velocity and the geometric dependency of the position of the laser beam relative to the main flow direction as outlined in Machefaux et al. (2012). This seems to be a suitable approach for small scan opening angles as in the measurement

https://doi.org/10.5194/wes-2019-89
Preprint. Discussion started: 4 December 2019
© Author(s) 2019. CC BY 4.0 License.

eawe european academy of wind energy
Open Access WIND ENERGY SCIENCE DISCUSSIONS

campaign presented here. Thus, the horizontal wind speed is defined as:

$$U(t) = U_{LOS} \cdot \frac{1}{\cos(\theta) \cdot \cos(\phi)} \tag{1}$$

with θ being the azimuth angle and ϕ the elevation angle of the LiDAR scan head.

4 Wind speed deficit in MFR calculation

The meandering time series and the wake's horizontal displacement are determined with the help of a Gaussian fit. Trujillo et al. (2011) assume that the probability of the wake position in vertical and horizontal direction is completely uncorrelated, so that the two-dimensional fitting function can be expressed as follows:

$$f_{2D} = \frac{A_{2D}}{2\pi\sigma_y\sigma_z} \exp\left[-\frac{1}{2}\left(\frac{(y_i-\mu_y)^2}{\sigma_y^2} + \frac{(z_i-\mu_z)^2}{\sigma_z^2}\right)\right] \tag{2}$$

with σ_y and σ_z being the standard deviations of the horizontal and vertical displacements μ_y and μ_z, respectively. In the analysis presented here only results from a horizontal line scan are analyzed, so that no vertical meandering is considered and the measurement results are fitted to a one-dimensional Gaussian curve defined as follows:

$$f_{1D} = \frac{A_{1D}}{\sqrt{2\pi}\sigma_y} \exp\left(-\frac{1}{2}\frac{(y_i-\mu_y)^2}{\sigma_y^2}\right), \tag{3}$$

where A_{1D} represents a scaling parameter. The measured wind speeds are fitted to the Gauss shape via a least-squares method. Thereby, only fitted horizontal displacements μ_y that are in between -200 m and 200 m are used for further validations of the mean wind speed in the MFR. A horizontal displacement of more than 200 m cannot be represented by the Gauss fit due to a lack of measurement points. However, such an event is highly improbable. Generally, this method of finding the wake position has proved to be very robust during the whole measurement campaign.

The entire method of calculating the wind speed deficit in the MFR is illustrated in Figure 2 and can be described as follows: The LiDAR system takes measurements from the nacelle of the turbine in downstream direction, which deliver the wind speed deficit in the nacelle frame of reference or even in the FFR (see left side of Figure 2) if the turbine is not moving (this can be ensured by the GPS systems). A Gauss curve is then fitted into the scanned points as explained previously. It provides the horizontal displacement of the wake, so that each scan point can be transferred into the MFR with the calculated displacement (see middle diagrams in Figure 2). The last step illustrated in the diagrams is the interpolation to a regular grid. These three steps are repeated for a certain number of scans N (e.g., approx. 37 for a 10-min time series). Finally, the mean value of all single measurement results in the MFR is calculated. It should be noted that it is mandatory to interpolate to a regular grid. Otherwise it would not be possible to take the mean of all scans since the horizontal displacement differs at each instant in time and, thereupon, the measurement points are transmitted to a different location in the MFR. After averaging, the plausibility of the results is inspected. If the calculated minimum mean wind speed in the MFR is higher than the minimum mean wind speed in the FFR, it is assumed that the Gauss fit failed and the results are no longer considered.

https://doi.org/10.5194/wes-2019-89
Preprint. Discussion started: 4 December 2019
© Author(s) 2019. CC BY 4.0 License.

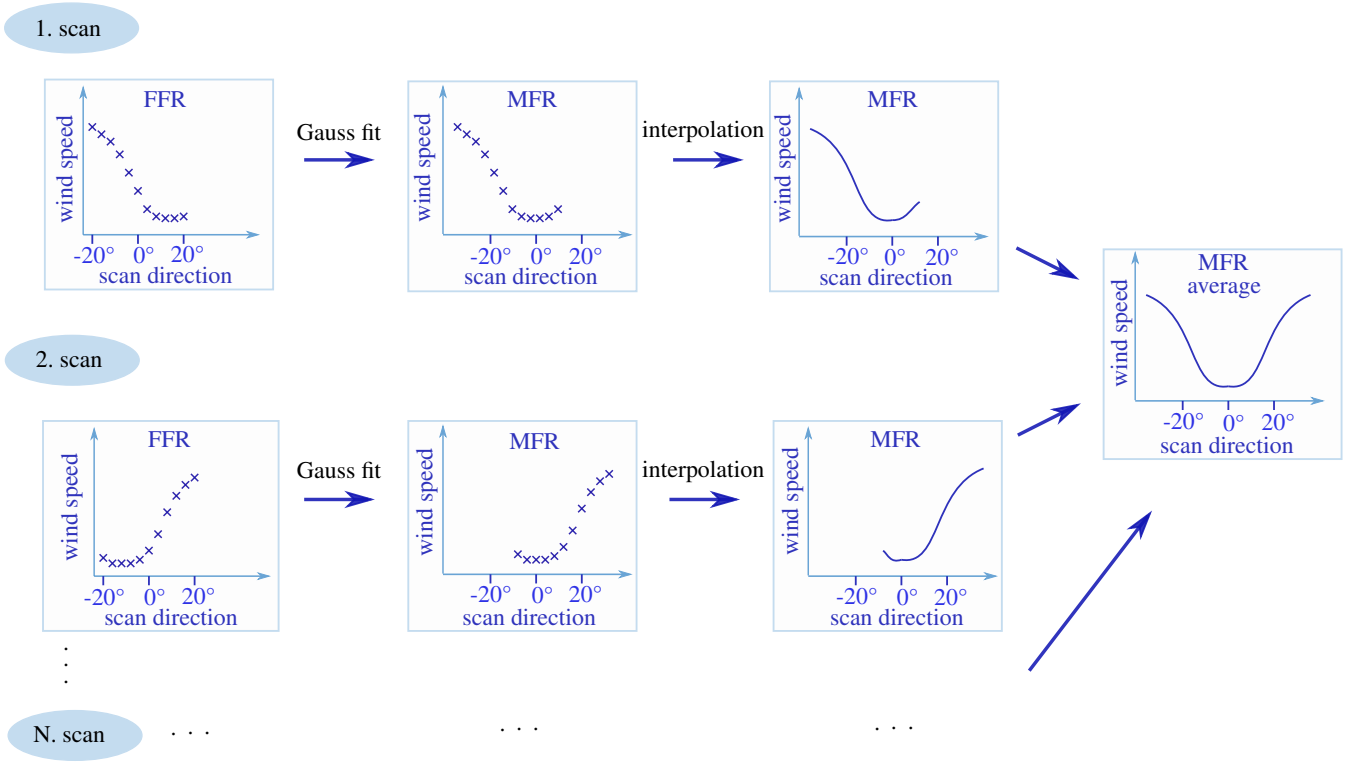

Figure 2. Method for the determination of the mean wind speed deficit in the MFR.

5 LiDAR simulation

One of the most challenging parts of this specific measurement campaign is the low ray update rate of the LiDAR system, which is considerably smaller than in the previously introduced measurement campaigns (see Bingöl et al. (2010) and Trujillo et al. (2011)). The issue is compensated by an optimized scan pattern determined by LiDAR and wind field simulations. The simulations incorporate LiDAR specifications (e.g. beam update rate and scan head angular velocity) and wind farm site conditions (ambient turbulence intensity and wind shear). The simulated LiDAR "takes measurements" in a simulated wind field that is generated by the DWM model and includes wake effects. A detailed description of the model is given in Section 6. From these "measured" wind speeds the meandering is determined via Gaussian fits as previously explained and implemented in the real measurement campaign. Simulations are performed for different scan patterns, ambient conditions and downstream distances to find an optimal scan pattern, which for this one-dimensional scan consists of only 11 scan points scanned in a horizontal line from $-20°$ to $20°$ in $4°$ steps.

In addition to the determination of the position of the wind speed deficit, the shape of the wind speed deficit in the MFR has also been estimated. The "measurement" results of the simulated meandering time series are shown in Figure 3(a), whereas the corresponding wind speed deficit in the MFR is presented in Figure 3(b). The results are compared to the original meandering

https://doi.org/10.5194/wes-2019-89
Preprint. Discussion started: 4 December 2019
© Author(s) 2019. CC BY 4.0 License.

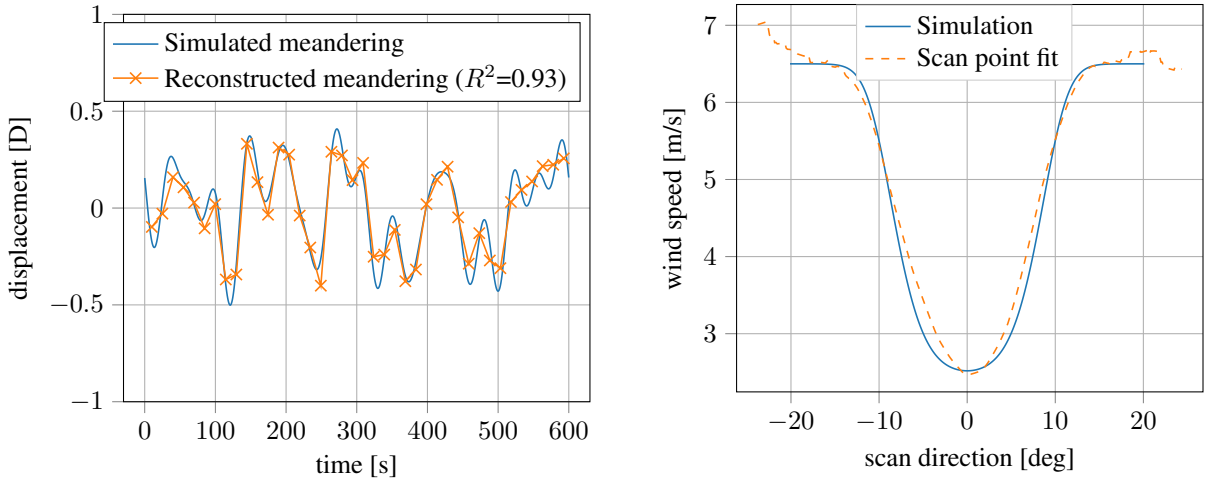

(a) (b)

Figure 3. Simulated and simulated "measured" meandering time series (a) and wind speed deficit in the MFR (b) at an ambient wind speed of 6.5 m/s.

time series and the simulated wind speed deficit. The "measured" wind speed deficit in the simulated environment reproduces the simulated wind speed and its underlying meandering time series very well. Although only 11 scan points are used for these plots, the curve of the wind speed deficit is very smooth. The reason for this behavior is the previously mentioned interpolation process. The distribution generated by the meandering process provides many scan points around the center of the wind speed deficit and only a few at the tails. Therefore, the influence of turbulence at the tails is much higher, leading to a somewhat coarse distribution at the boundaries of the deficit. It should also be noted that since this is a one-dimensional scan, the simulated LiDAR "measures" the wind speed deficit only horizontally neglecting the wake's less dominant vertical movement. Whenever the wind speed deficit is mentioned in subsequent validations, it implies the neglection of the vertical meandering, which has only a marginal impact on the shape of the wind speed deficit in the FFR.

The LiDAR simulations indicate that the Gauss fit works more reliable under optimal operating conditions when the wind speed deficit is most pronounced. For the turbines examined, this applies in a range of 5 m/s up to 8 m/s, so that only measurement results with ambient wind speeds in this interval are analyzed.

6 Dynamic wake meandering model

The measured wind speed deficit in the MFR is consecutively compared to the DWM model, which is based on the assumption that the wake behaves as a passive tracer in the turbulent wind field. Consequently, the movement of the passive structure, i.e. the wake deficit, is driven by large turbulence scales (Larsen et al. (2007) and Larsen et al. (2008b)). The main components of the model are summarized in Figure 4(a).

https://doi.org/10.5194/wes-2019-89
Preprint. Discussion started: 4 December 2019
© Author(s) 2019. CC BY 4.0 License.

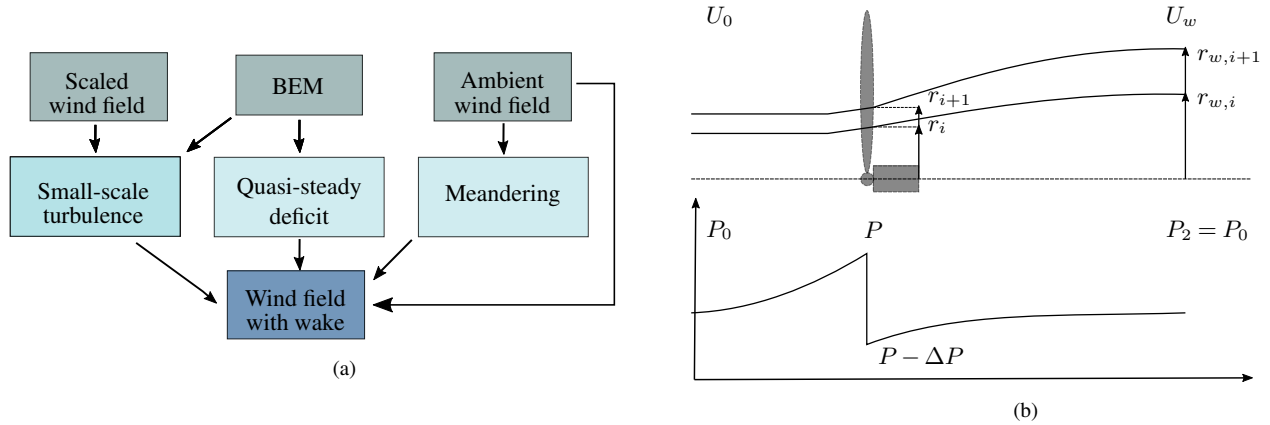

Figure 4. Components of the DWM model (a) (Reinwardt et al., 2018) and schematic illustration of the wake expansion in the DWM model (b) according to Madsen et al. (2010).

6.1 Quasi-steady wake deficit

One key point of the model is the quasi-steady wake deficit or rather the wind speed deficit in the MFR. It compares directly to the LiDAR measurements after transforming the measurements into the MFR as explained in the last section. In this study, two calculation methods for the quasi-steady wake deficit are compared with the LiDAR measurement results. A similar comparison of these models to metmast measurements in the FFR was published in Reinwardt et al. (2018). The quasi-steady wake deficit is defined in the MFR and consists of a formulation of the initial deficit emitted by the wake generating turbine and the expansion of the deficit downstream (Larsen et al., 2008a). The latter is calculated with the thin shear-layer approximation of the Navier-Stokes equations in its axisymmetric form. This method is strongly related to the work of Ainslie (1988) and outlined in Larsen et al. (2007). The thin shear-layer equations expressed by the wind speed in axial and radial direction U and V_r, respectively, are defined as follows:

$$U\frac{\partial U}{\partial x} + V_r\frac{\partial U}{\partial r} = \frac{1}{r}\frac{\partial}{\partial r}\left(\nu_T r\frac{\partial U}{\partial r}\right) \tag{4}$$

$$\frac{1}{r}\frac{\partial}{\partial r}(rV_r) + \frac{\partial U}{\partial x} = 0 \tag{5}$$

The first part of the quasi-steady wake deficit, the initial deficit, serves as a boundary condition when solving the equations. In both methods used to determine the quasi-steady wake deficit, the initial deficit is based on the axial induction factor derived from the blade element momentum (BEM) theory. Pressure terms in the thin shear-layer equations are neglected. The error that inherently comes with this assumption is accommodated by using the wind speed deficit two rotor diameters downstream (beginning of the far-wake area) as a boundary condition for the solution of the thin shear-layer equations. The equations are solved by a finite-differences method combined with an eddy viscosity (ν_T) closure approach. The two methods that are compared with the LiDAR measurements only differ in the definition of the initial deficit and the eddy viscosity formulation.

https://doi.org/10.5194/wes-2019-89
Preprint. Discussion started: 4 December 2019
© Author(s) 2019. CC BY 4.0 License.

eawe european academy of wind energy
Open Access WIND ENERGY SCIENCE DISCUSSIONS

6.1.1 DWM-Egmond

For the first method the following formulae are given to calculate the initial deficit. Hence, the boundary condition for solving the thin shear-layer equations are (Madsen et al., 2010):

$$U_w\left(\frac{r_{w,i+1}+r_{w,i}}{2}\right) = U_0(1-2a_i) \tag{6}$$

and

$$r_{w,i+1} = \sqrt{\frac{1-a_i}{1-2a_i}\left(r_{i+1}^2 - r_i^2\right) + r_{w,i}^2}\, f_w \tag{7}$$

with

$$f_w = 1 - 0.45\bar{a}^2, \tag{8}$$

where $\bar{a}$ represents the mean induction factor along all radial positions i, r_i the rotor radius and $r_{w,i}$ the wake radius. The boundary condition of the radial velocity component is $V_r = 0$. The initial wake expansion and the corresponding radial positions as well as the pressure recovery in downstream direction are illustrated in Figure 4(b). The eddy viscosity ν_T used in equation (4), is calculated in this first approach as follows (Larsen et al., 2013):

$$\frac{\nu_T}{U_0 R} = k_1 F_1(\tilde{x}) F_{amb}(\tilde{x}) I_0 + k_2 F_2(\tilde{x}) \frac{R_w(\tilde{x})}{R}\left(1 - \frac{U_{min}(\tilde{x})}{U_0}\right) \tag{9}$$

with $k_1 = 0.1$ and $k_2 = 0.008$. The eddy viscosity is normalized by the ambient wind speed U_0 and the rotor radius R. The outlined definition consists of two terms. The first is related to the ambient turbulence intensity I_0, whereas the second depends on the shape of the wind speed deficit itself. The single terms are weighted with the factors k_1 and k_2. The filter functions F_1 and F_2 in equation (9) depending on $\tilde{x}$ (downstream distance normalized by the rotor radius) are defined by IEC 61400-1 Ed.4 as follows:

$$F_1(\tilde{x}) = \begin{cases} \left(\frac{\tilde{x}}{8}\right)^{3/2} - \frac{\sin\left(\frac{2\pi\tilde{x}^{3/2}}{8^{3/2}}\right)}{2\pi} & \text{for } 0 \le \tilde{x} < 8 \\ 1 & \text{for } \tilde{x} \ge 8 \end{cases} \tag{10}$$

$$F_2(\tilde{x}) = \begin{cases} 0.0625 & \text{for } 0 \le \tilde{x} < 4 \\ 0.025\tilde{x} - 0.0375 & \text{for } 4 \le \tilde{x} < 12 \\ 0.00105(\tilde{x}-12)^3 + 0.025\tilde{x} - 0.0375 & \text{for } 12 \le \tilde{x} < 20 \\ 1 & \text{for } \tilde{x} \ge 20 \end{cases} \tag{11}$$

The filter function F_2 covers the lack of equilibrium between the velocity field and the rising turbulence in the beginning of the wake. F_1 is introduced to include the fact that the depth of the wind speed deficit increases in the near-wake area up to (2...3)D downstream of the turbine until it attenuates again in downstream direction (Madsen et al., 2010). A more detailed explanation of the nonlinear coupling function F_{amb} is given in Section 6.4. This calculation method (equations (6) to (11)) is subsequently named “DWM-Egmond” after the site, which is used for the calibration of the eddy viscosity in Larsen et al. (2013).

https://doi.org/10.5194/wes-2019-89
Preprint. Discussion started: 4 December 2019
© Author(s) 2019. CC BY 4.0 License.

eawe european academy of wind energy
Open Access WIND ENERGY SCIENCE DISCUSSIONS

6.1.2 DWM-Keck

The second investigated method defines the initial deficit by the following equations (Keck, 2013):

$$U_w(r_{w,i}) = U_0\,(1-(1+f_u)\,a_i) \tag{12}$$

$$r_{w,i} = r_i\sqrt{\frac{1-\bar{a}}{1-(1+f_R)\,\bar{a}}} \tag{13}$$

with $f_u = 1.1$ and $f_R = 0.98$. The boundary condition of the radial velocity component is again $V_r = 0$. In Keck (2013) the final and recommended version of the model developed for the eddy viscosity is defined as follows:

$$\nu_T = k_1 F_1(\tilde{x})\; u^*_{ABL;\lambda<2D}\; l^*_{ABL;\lambda<2D} + k_2 F_2(\tilde{x}) \max\left(l^{*2}\left|\frac{\partial U(\tilde{x})}{\partial r}\right|, l^*\,(1-U_{min}(\tilde{x}))\right) \tag{14}$$

with $k_1 = 0.578$ and $k_2 = 0.0178$ and the filter functions:

$$F_1 = \begin{cases} \frac{\tilde{x}}{4} & \text{for } \tilde{x} < 4 \\ 1 & \text{for } \tilde{x} \geq 4 \end{cases} \tag{15}$$

and

$$F_2 = \begin{cases} 0.035 & \text{for } \tilde{x} < 4 \\ 1 - 0.965e^{-0.35(\tilde{x}/2-2)} & \text{for } \tilde{x} \geq 4 \end{cases} \tag{16}$$

In contrast to the previously mentioned model (DWM-Egmond) atmospheric stability is considered in this final model description. Equation (14) involves the velocity $u^*_{ABL;\lambda<2D}$ and length scale $l^*_{ABL;\lambda<2D}$ fractions of the ambient turbulence, which is related to the wake deficit evolution (eddies smaller than 2D). The velocity scale $u^*_{ABL;\lambda<2D}$ is besides the ambient turbulence intensity I_0 related to the ratio of the Reynolds stresses (normal stress in flow direction and the shear stress), which in turn are functions of atmospheric stability. A detailed description of a method to introduce atmospheric stability in the DWM model can be found in Keck et al. (2014) and Keck (2013). In contrast to the final and recommended model in Keck (2013), atmospheric stability is not considered in this study, so that a previous model in Keck (2013) without consideration of atmospheric stability is used and the numerical constants k_1 and k_2 in equation (17) are changed with respect to the first least-squares recalibration in Keck (2013). Furthermore, according to Keck (2013) it can be assumed that the mixing length l^* is equal to half of the wake width. This results in following formulation of the eddy viscosity:

$$\frac{\nu_T}{U_0 R} = k_1 F_1(\tilde{x}) I_0 + k_2 F_2(\tilde{x}) \max\left(\frac{R_w(\tilde{x})^2}{R U_0}\left|\frac{\partial U(\tilde{x})}{\partial r}\right|, \frac{R_w(\tilde{x})}{R}\left(1-\frac{U_{min}(\tilde{x})}{U_0}\right)\right) \tag{17}$$

with $k_1 = 0.0914$ and $k_2 = 0.0216$.

https://doi.org/10.5194/wes-2019-89
Preprint. Discussion started: 4 December 2019
© Author(s) 2019. CC BY 4.0 License.

6.2 Meandering of the wake

The meandering of the wind speed deficit is calculated from the large turbulence scales of the ambient turbulent wind field. Thus, the vertical and horizontal movements are calculated from an ideal low-pass filtered ambient wind field. The cut-off frequency of the low-pass filter is specified by the ambient wind speed and the rotor radius as (Larsen et al., 2013):

$$f_c = \frac{U_0}{4R} \tag{18}$$

The horizontal $y(t)$ and vertical $z(t)$ positions of the wind speed deficit are calculated based on the low-pass filtered velocoties in horizontal and vertical directions according to the relations (Larsen et al., 2007):

$$\frac{\mathrm{d}y(t)}{\mathrm{d}t} = v(t) \tag{19}$$

and

$$\frac{\mathrm{d}z(t)}{\mathrm{d}t} = w(t), \tag{20}$$

where $v(t)$ and $w(t)$ are the fluctuating wind speeds at hub height. The ambient wind field, which is later on low-pass filtered, is generated in this work by a Kaimal spectrum and a coherence function (e.g., Veers, 1988).

6.3 Small-scale turbulence

Another aspect of the DWM model is the definition of the small-scale turbulence generated through the wake shear itself as well as blade tip and root vortices. This part of the turbulence is calculated with a scaled homogeneous turbulent wind field also generated by a Kaimal spectrum. The scaling factor k_{aw} is defined by (IEC 61400-1 Ed.4):

$$k_{aw}(\tilde{x},\tilde{r}) = 0.6\left|1-\tilde{U}(\tilde{x},\tilde{r})\right| + 0.35\left|\frac{\partial\tilde{U}(\tilde{x},\tilde{r})}{\partial\tilde{r}}\right| \tag{21}$$

Equation (21) uses the normalized wind speed deficit $\tilde{U}(\tilde{x},\tilde{r})$ based on the calculation of the initial deficit, which itself builds on the BEM theory and the aerodynamics of the turbine. This study analyzes only the mean wind speed in the MFR and the meandering itself. Therefore, the analysis of the small-scale turbulence is not part of the validation. Nevertheless, for the sake of completeness of the model is mentioned at this point.

6.4 Recalibration of the DWM model

The wind speed deficit measured by the LiDAR systems is used to recalibrate the wake degradation downstream or to be more precise the eddy viscosity description. In Larsen et al. (2013) a recalibration was already achieved by introducing a nonlinear coupling function F_{amb} into the ambient turbulence intensity term of the eddy viscosity definition (see equation (9)). Furthermore, a comparison between the measured and simulated power based on the DWM model was carried out. It shows that for lower turbulence intensities and moderate to high turbine distances the wind speed deficit degradation is too low. For this reason the function F_{amb} depending on the downstream distance was introduced into the eddy viscosity description.

https://doi.org/10.5194/wes-2019-89
Preprint. Discussion started: 4 December 2019
© Author(s) 2019. CC BY 4.0 License.

eawe european academy of wind energy
Open Access WIND ENERGY SCIENCE DISCUSSIONS

A similar behavior but even more pronounced can be seen in the results in Section 7. Following the approach of Larsen et al. (2013), a function based on a least-squares calibration with the acquired LiDAR measurements is developed. This function is incorporated into the normalized eddy viscosity description in eq. (17), whereby it changes to:

$$\frac{\nu_T}{U_0 R} = k_1 F_{amb}(\tilde{x}) F_1(\tilde{x}) I_0 + k_2 F_2(\tilde{x}) \max\left(\frac{R_w(\tilde{x})^2}{R U_0} \left| \frac{\partial U(\tilde{x})}{\partial r} \right|, \frac{R_w(\tilde{x})}{R} \left(1 - \frac{U_{min}(\tilde{x})}{U_0} \right) \right) \tag{22}$$

with the constants $k_1 = 0.0924$ and $k_2 = 0.0216$ and the coupling function

$$F_{amb}(\tilde{x}) = a\tilde{x}^{-b} \tag{23}$$

with $a = 0.285$ and $b = 0.742$. The parameters a and b are the results of the least-squares calibration. It should be noted that the constant k_1 was also slightly adjusted by the recalibration, in which the normalized eddy viscosity definition of Keck (2013) has been used. The reason for that is that this model is already in relatively good agreement with the measurement results as demonstrated in Section 8 and also in Reinwardt et al. (2018).

7 Measurement results

The measurement campaign lasted from January to July 2019. Both LiDAR systems, introduced in Section 2, were used to collect the data. Results of the meandering time series over 10 minutes are exemplarily shown in Figure 5(a). The maximum

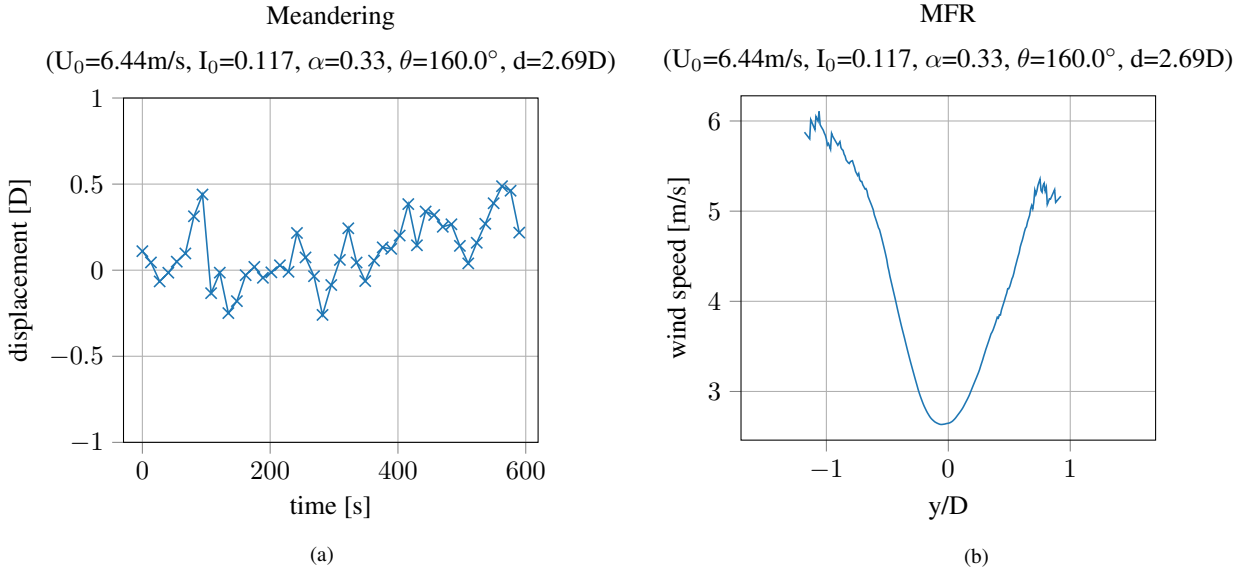

(a) (b)

Figure 5. Meandering time series **(a)** and wind speed deficit in the MFR **(b)** at 2.69D downstream of the turbine.

displacement of the wake is about 0.5D, which is equivalent to 58.5 m. The results are derived from a 10-min time series with an ambient wind speed of 6.44 m/s and an ambient turbulence intensity of 11.7%. Some of the metmast detected ambient

https://doi.org/10.5194/wes-2019-89
Preprint. Discussion started: 4 December 2019
© Author(s) 2019. CC BY 4.0 License.

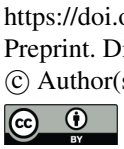

eawe european academy of wind energy
Open Access WIND ENERGY SCIENCE DISCUSSIONS

conditions (wind speed U_0, turbulence intensity I_0, wind shear α and wind direction θ) are given in the title of the figure. The corresponding mean wind speed deficit is illustrated in Figure 5(b). The wind speed decreases to less than 3 m/s in full wake situations. As explained in Section 5, the tails of the curve are relatively coarse since less scan points were gathered. It can also be seen that the ambient wind speed is not even reached at the edges of the curve. The opening angle of the scan appears too small to capture the whole wake at this distance. Towards the left part of the wind speed deficit (at negative y distances) a bigger part of the wake is captured. This arises from the fact that the horizontal displacement is more often positive than negative and, therefore, more measurement results are collected towards the left part of the wind speed deficit curve.

The used LiDAR system is capable of measuring several range gates simultaneously in 30 m intervals. The results of all detected range gates for the data set presented in Figure 5 are shown in Figure 6(a). The closest distance is 1.92D downstream

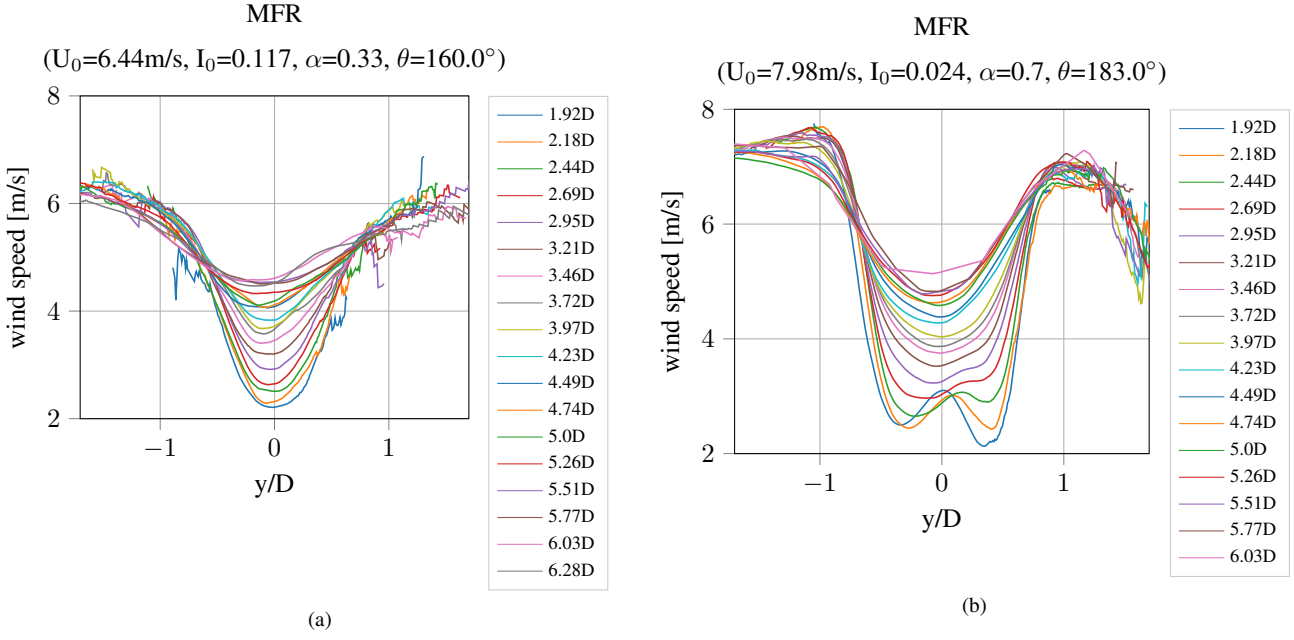

Figure 6. Wind speed deficit in MFR for an ambient turbulence intensity of 11.7% **(a)** and a turbulence intensity of 2.4% **(b)**.

and the farthest is 6.28D. The degradation of the wind speed deficit in downstream direction is clearly identifiable. As for the single distance case (Figure 5), for most range gates a bigger database is captured at the left part of the wind speed deficit, resulting in smoother curves. The presumption of a too small opening angle of the scan, as stated before, proves true. With increasing downstream distances the captured wind speed deficits get closer to integrity. A broader scan angle would result in more detailed wind speed deficits for close downstream distances at the expense of far distances, where the scan points might not capture enough points inside the deficit and thereby prevent a successful Gaussian fit. Furthermore, additional scan points at the edges can lead to a better representation of the deficit but would also increase the scan time.

https://doi.org/10.5194/wes-2019-89
Preprint. Discussion started: 4 December 2019
© Author(s) 2019. CC BY 4.0 License.

eawe european academy of wind energy
Open Access WIND ENERGY SCIENCE DISCUSSIONS

Figure 6(b) illustrates the wind speed deficit in the MFR measured under different ambient conditions. The corresponding meandering time series and wind speed deficit for this measured time series at 2.96D downstream is given in Figure A1 in the appendix. The wind shear is fairly high ($\alpha = 0.7$) and the turbulence intensity is very low ($I_0 = 2.4\%$). Due to the low turbulence intensity it is still possible to see the w-shape of the wind speed deficit at closer distances. The typical w-shape is caused by the low axial induction in the area of the nacelle. Further downstream, the wake becomes more Gaussian shaped. At a horizontal distance of about 1.5D from the wake center, the wind speed decreases. The reason is probably the wake of other turbines in the wind farm. The mean wind direction in this time series is $183°$ and the measurements are taken from WTG 1, so it could be either the influence of the wakes of WTG 2 or WTG 4. The associated results of the mean wind speed deficit in the FFR are illustrated in Figure 7. The curves in the FFR are less smooth than the wind speed deficit in the MFR, simply because only 11 points are scanned and no interpolation is necessary when calculating the mean wind speed over the whole time series. Comparing Figures 6 and 7, it becomes apparent that the wind speed deficit in the FFR is less pronounced. Furthermore, for the lower turbulence intensity the w-shape of the wind speed is not visible, since it vanished due to the meandering.

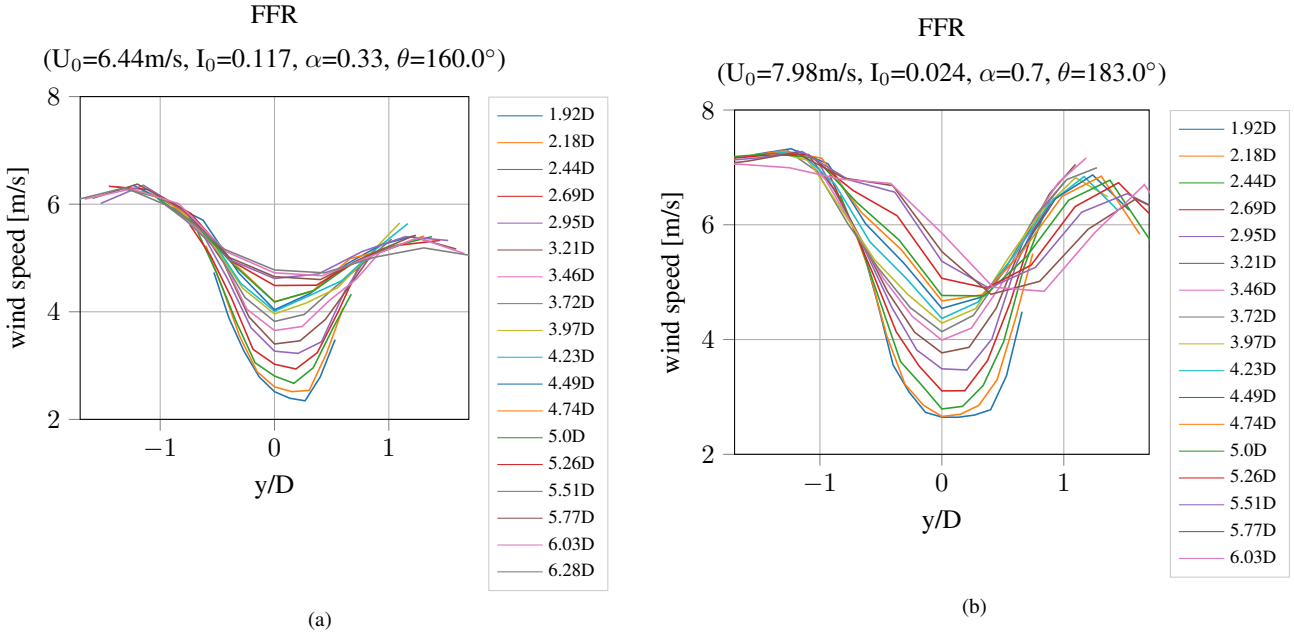

Figure 7. Wind speed deficit in FFR for a turbulence intensity of 11.7% **(a)** and a turbulence intensity of 2.4% **(b)**.

Similar results as exemplarily shown in Figures 6 and 7 have been collected for a multitude of different ambient conditions. The number of measured time series per turbulence intensity and wake generating turbine, on which the LiDAR system is installed, is listed in Table 2. The turbulence intensity is binned in 2° steps. Column 1 of Table 2 specifies the mean values for each bin. Most of the measurement results are collected at low to moderate turbulence intensities ($I_0 = (4...10)\%$). Only a few results could be extracted at higher turbulence intensities. The results include time series with an ambient wind speed of 5 m/s to 8 m/s. In this range both turbines operate under optimal and most efficient conditions resulting in maximum energy

https://doi.org/10.5194/wes-2019-89
Preprint. Discussion started: 4 December 2019
© Author(s) 2019. CC BY 4.0 License.

eawe european academy of wind energy
Open Access WIND ENERGY SCIENCE DISCUSSIONS

Table 2. Number of measured and considered data sets per turbulence intensity for the LiDAR systems on WTG 1 and WTG 2

I_0 [%]	WTG 1	WTG 2
4	23	28
6	8	11
8	23	14
10	11	9
12	13	4
14	0	0
16	1	1
18	1	2
20	1	3
22	0	2

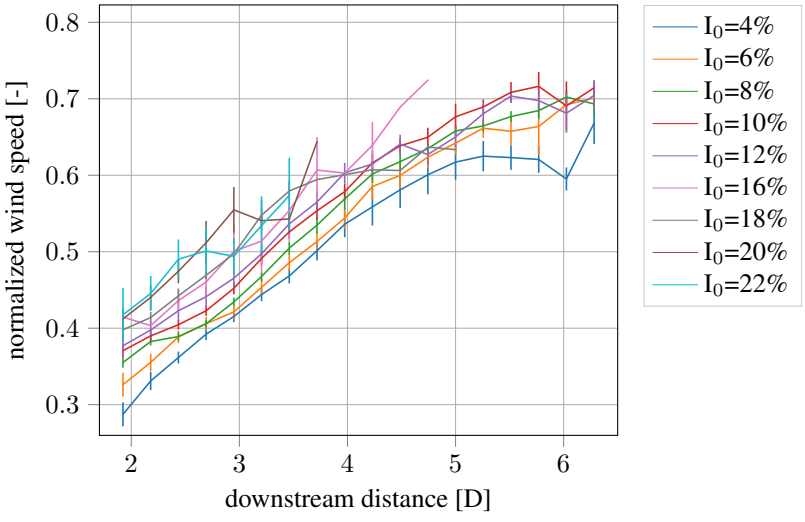

Figure 8. Measured mean value (line) and standard deviation of the mean value (bar) of the minimal wind speed in the MFR for different turbulence intensity bins with a bin width of 2%

output from the wind. The thrust coefficient is constant in this region. Therefore, the axial induction and the wind speed deficit normalized by the turbine's inflow wind speed are also expected to be constant for similar ambient conditions over this wind speed range.

Figure 8 summarizes all measured wind speed deficits in the MFR. It demonstrates the mean value and the standard deviation of the mean for all captured turbulence bins plotted against the downstream distance. Each value is related to the minimum value of the wind speed deficit, which itself is normalized by the inflow wind speed. It should be noted that in some distances only one value satisfies the filtering and plausibility checks, whereby the error bar is omitted. Additionally, it is pointed out that the plotted values always refer to the minimum value of a wind speed curve and not necessarily to the velocity in the wake center. Therefore, no increase of the wind speed at low downstream distances on account of the w-shape is visible. The wind speed deficit at the wake center plotted against the downstream distance is depicted in the next section in Figure 10(b) and will be discussed further at this point. Figure 8 illustrates very well that the lowest degradation of the wind speed deficit occurs at the lowest turbulence intensity. Up to a turbulence intensity of 10%, the degradation of the wind speed deficit continuously rises, leading to increasing minimum wind speeds at nearly all downstream distances. Above 10% turbulence intensity, the case is less clear. Especially at larger downstream distances, the measured normalized minimum wind speed happens to fall below the corresponding lower turbulence intensity bin. The most obvious explanation is the reduced number of measurement results in these bins and the higher uncertainty that comes along with it (expressed as error bars). Furthermore, discrepancies in the determined ambient turbulence intensity at the metmast location and the actual turbulence intensity at the wake position

https://doi.org/10.5194/wes-2019-89
Preprint. Discussion started: 4 December 2019
© Author(s) 2019. CC BY 4.0 License.

could lead to an misinterpretation of the LiDAR measurements. Nevertheless, even though there are some discrepancies, the faster recovery of the wind speed deficit due to the higher ambient turbulence intensity can be verified. Thus, it is valid to use these measurement results for a comparison and a recalibration of the DWM model in the next section.

8 Comparison between measurements and DWM model simulation

Figure 9 compares the measured normalized minimum wind speed in the wake to DWM model simulations. The left part of Figure 9 shows results for a relatively low turbulence intensity of 6%, whereas the right part contains results for a higher turbulence intensity of 16%. Further results for the remaining turbulence intensity bins are shown in Figures B1 and B2 in the appendix. The simulations were carried out for a specific downstream distance, which corresponds to the center of the range gate of the LiDAR system. It should be noted that the measured wind speeds with the LiDAR system can be interpreted as a mean value over the whole range gate. However, the wind speed gradient in axial direction is relatively low and almost linear in the observed donstream distances, so that a fair comparison between simulation and measurements is carried out. Three different simulation results with varying definitions of the initial deficit and eddy viscosity description are illustrated. The method called “DWM-Egmond” is based on the definitions from Madsen et al. (2010) and Larsen et al. (2013) and the “DWM-Keck” method is adopted from Keck (2013), see Section 6. It is obvious that the DWM-Egmond method overestimates the wind speed deficit over all downstream distances for both turbulence intensities. The simulated minimum wind speed with the DWM-Keck method is in better agreement with the measurement results. This confirms the results in Reinwardt et al. (2018). Especially at higher turbulence intensities (Figure 9(b)), the results of the DWM-Keck model agree very well with the measurements. For lower turbulence intensities and higher distances (greater than 3D) there is a relatively large discrepancy between measurements and simulations. A similar observation was made in Larsen et al. (2013). Aiming at the adjustment of the simulated degradation of the wind speed deficit for cases like the one presented here, the DWM model has been recalibrated and henceforth called “DWM-Keck-c” (see Figure 9).

The recalibration of the DWM model and accordingly the normalized eddy-viscosity definition in the DWM model are based on a least-squares fit of the minimum of the simulated normalized wind speed to the minimum of the measured normalized wind speed for several downstream distances. The definition of the eddy viscosity along with the recalibrated parameters are explained in detail in Section 6.4. For the recalibration the measurement results are divided into 2% turbulence intensity bins. All measurement results from Figure 8 containing data sets from two different turbines, are used for the recalibration. The first turbine is an N117 turbine with 3 MW and the second one is an N117 with 2.4 MW. DWM model simulations were carried out for both turbine types due to the fact that the axial induction of both turbines is slightly different under partial load conditions. To calculate a mean value of the simulated minimum wind speed and thus allow a comparison with the results in Figure 8, the simulation results are weighted in accordance with the number of measurement results per turbine listed in Table 2. The results of the recalibrated DWM model, denoted Keck-c in Figure 9, coincide very well with the measurements. In particular, the results for lower turbulence intensities could clearly be improved. For higher turbulence intensities, the influence

https://doi.org/10.5194/wes-2019-89
Preprint. Discussion started: 4 December 2019
© Author(s) 2019. CC BY 4.0 License.

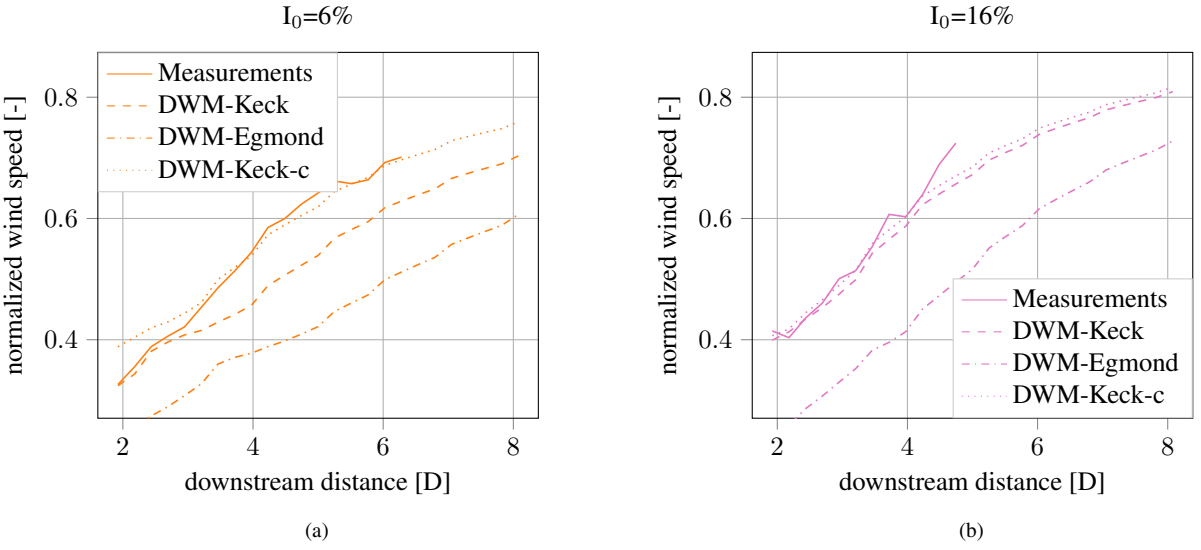

Figure 9. Comparison of measurements and simulations of the minimum wind speed deficit in the MFR for different downstream distances. The recalibrated model is denoted DWM-Keck-c.

of the recalibration is less significant and the already good agreement between simulation and measurement results remains unchanged. The same applies to the results in the appendix in Figures B1 and B2.

Figure 10 compares the final recalibrated DWM model to the original model definition. It shows the minimum normalized wind speed (a) and the wind speed at the wake center (b) over downstream distances from 0D to 10D for the lower and the higher turbulence intensity cases of 6% and 16%, respectively. Observing the wind speed at the wake center, higher wind speeds can be seen at lower distances, which derives from the w-shape of the wind speed at these downstream distances. The comparison of the DWM-Keck model (orange curve) and the recalibrated model DWM-Keck-c (green curve) demonstrates that the recalibration leads to a shift of the curve towards lower distances. This shift is more pronounced for the lower turbulence intensity, leading to a faster degradation of the wind speed deficit. For the higher turbulence intensity, both curves, orange and green, are very close to each other over all distances. Contemplating the curve of the minimum wind speed in Figure 10(a), small steps are formed in the curves between 2D and 4D (depending on the used model and the turbulence intensity). These steps correspond to the minimum of the curves in Figure 10(b) and are thus related to the transition from the w-shape of the wind speed deficit towards the Gaussian profile and are consequently caused by the resolution in downstream direction. These steps, visible in Figure 10(a), were also found in some measurements and could likewise be related to the implied transition zone.

https://doi.org/10.5194/wes-2019-89
Preprint. Discussion started: 4 December 2019
© Author(s) 2019. CC BY 4.0 License.

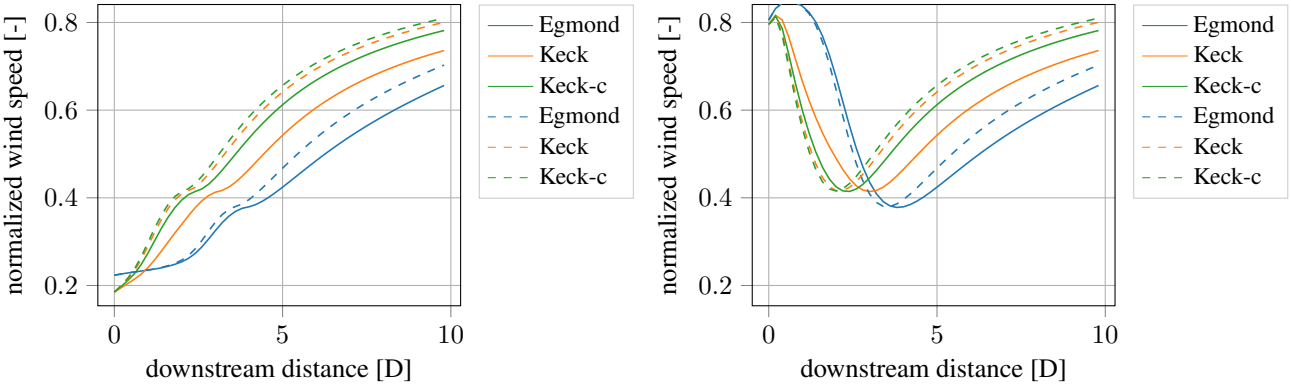

(a) (b)

Figure 10. Simulated minimal normalized wind speed in the MFR **(a)** and normalized wind speed at the wake center **(b)** over the downstream distance for a turbulence intensity of 6% (solid curves) and 16% (dashed curves). The recalibrated model is denoted DWM-Keck-c.

9 Conclusions

The study compares measurements of the wind speed deficit with DWM model simulations. The measurement campaign consists of two nacelle mounted LiDAR systems in a densely packed onshore wind farm. The LiDAR measurements were prepared with LiDAR and wind field simulations to determine an optimal scan pattern. Several wind speed deficits that were simultaneously measured at different downstream distances are presented along with their associated meandering time series. The one-dimensional scan worked reliably in the field campaign, thus, delivering LiDAR data for a multitude of different ambient conditions. These measurements are compared to the simulated wind speed deficit in the MFR. The simulation result of the DWM-Keck model is in good agreement, whereas the DWM-Egmond model yields a too low degradation of the wind speed deficit. Furthermore, even the DWM-Keck model shows some discrepancies to the measurements at low turbulence intensities, which is why a recalibrated DWM model was proposed. The recalibrated model improves the correlation with measurements at low turbulence intensities and leads to a comparably good agreement at high turbulence intensities like the original model, thus, resulting in a very well overall conformity with the measurements.

Future work will include the analysis of two-dimensional scans as well as measurements with more range gates and higher spatial resolutions. Increasing the number of range gates and scan points will lead to higher scan times, hence, preventing further analysis of the wind speed deficit in the MFR and the determination of the meandering time series. Nevertheless, a validation of the wind speed deficit in the FFR with higher resolutions and more distances seems reasonable to prove the validity of the outlined calibration also for further distances. Furthermore, the analyzed models will be assessd in load simulations and compared with the measured loads in the wind farm. So far, only measured single wakes were presented. Yet, a brief analysis

https://doi.org/10.5194/wes-2019-89
Preprint. Discussion started: 4 December 2019
© Author(s) 2019. CC BY 4.0 License.

eawe european academy of wind energy
Open Access WIND ENERGY SCIENCE DISCUSSIONS

demonstrated that multiple wakes can also be recorded with the described measurement setup. A future step will therefore be an analysis of multiple wake situations.

Code and data availability. Access to LiDAR and metmast data as well as the source code used for post-processing the data and simulations can be requested by the authors.

Author contributions. IR performed all simulations, post-processed and analyzed the measurement data and wrote the paper. LS and DS gave technical advice in regular discussions and reviewed the paper. PD and MB reviewed the paper and supervised the investigations.

Competing interests. The authors declare that they have no conflict of interest.

Acknowledgements. The content of this paper was developed within the project NEW 4.0 (North German Energy Transition 4.0), which is funded by the Federal Ministry for Economic Affairs and Energy (BMWI).

https://doi.org/10.5194/wes-2019-89
Preprint. Discussion started: 4 December 2019
© Author(s) 2019. CC BY 4.0 License.

eawe european academy of wind energy
Open Access WIND ENERGY SCIENCE DISCUSSIONS

Appendix A: Measurement results

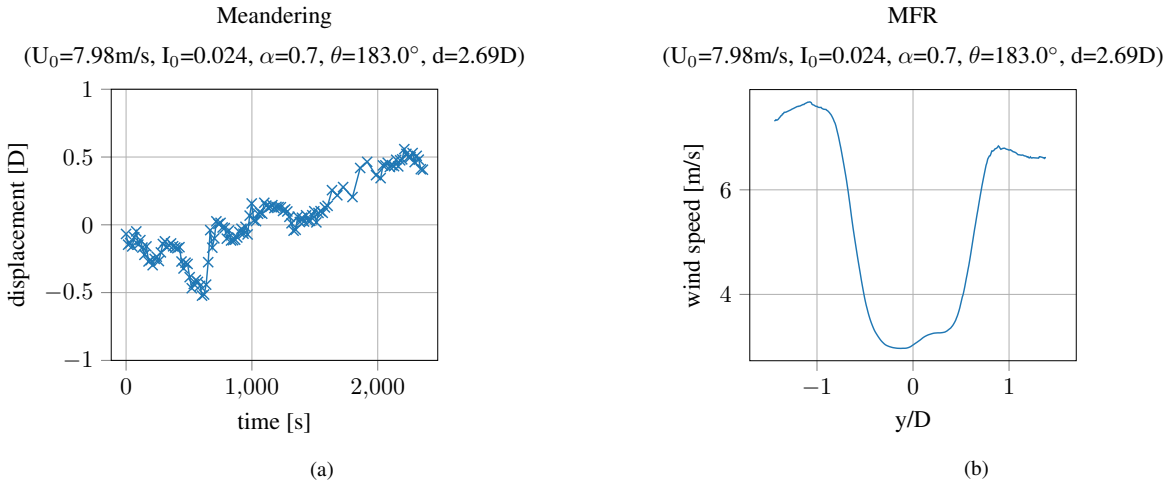

Figure A1. Meandering time series **(a)** and wind speed deficit in the MFR **(b)** at 2.69D downstream of the turbine.

Appendix B: Comparison of measurements and DWM model simulation

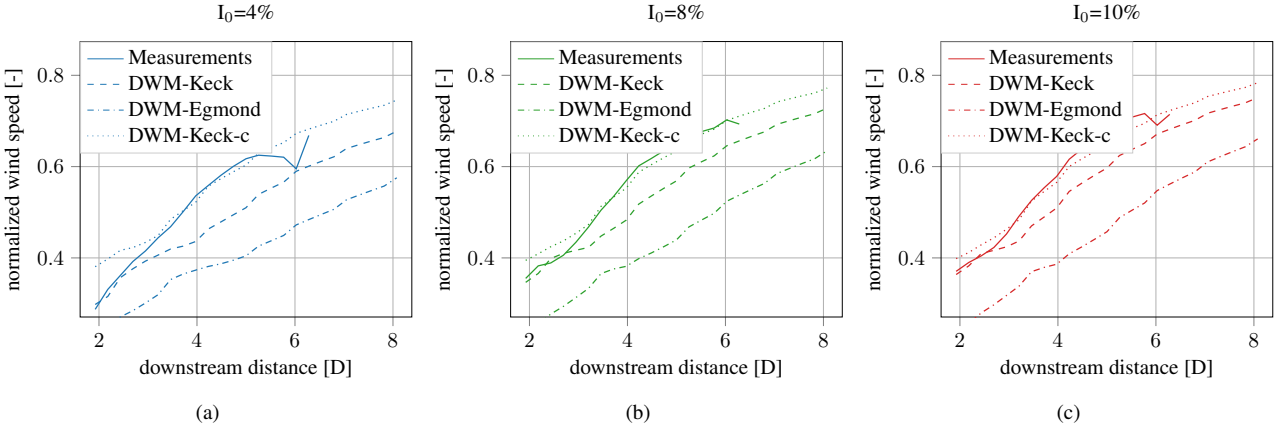

Figure B1. Comparison of measurements and simulations of the minimum wind speed deficit in the MFR for different downstream distances. The recalibrated model is denoted DWM-Keck-c.

https://doi.org/10.5194/wes-2019-89
Preprint. Discussion started: 4 December 2019
© Author(s) 2019. CC BY 4.0 License.

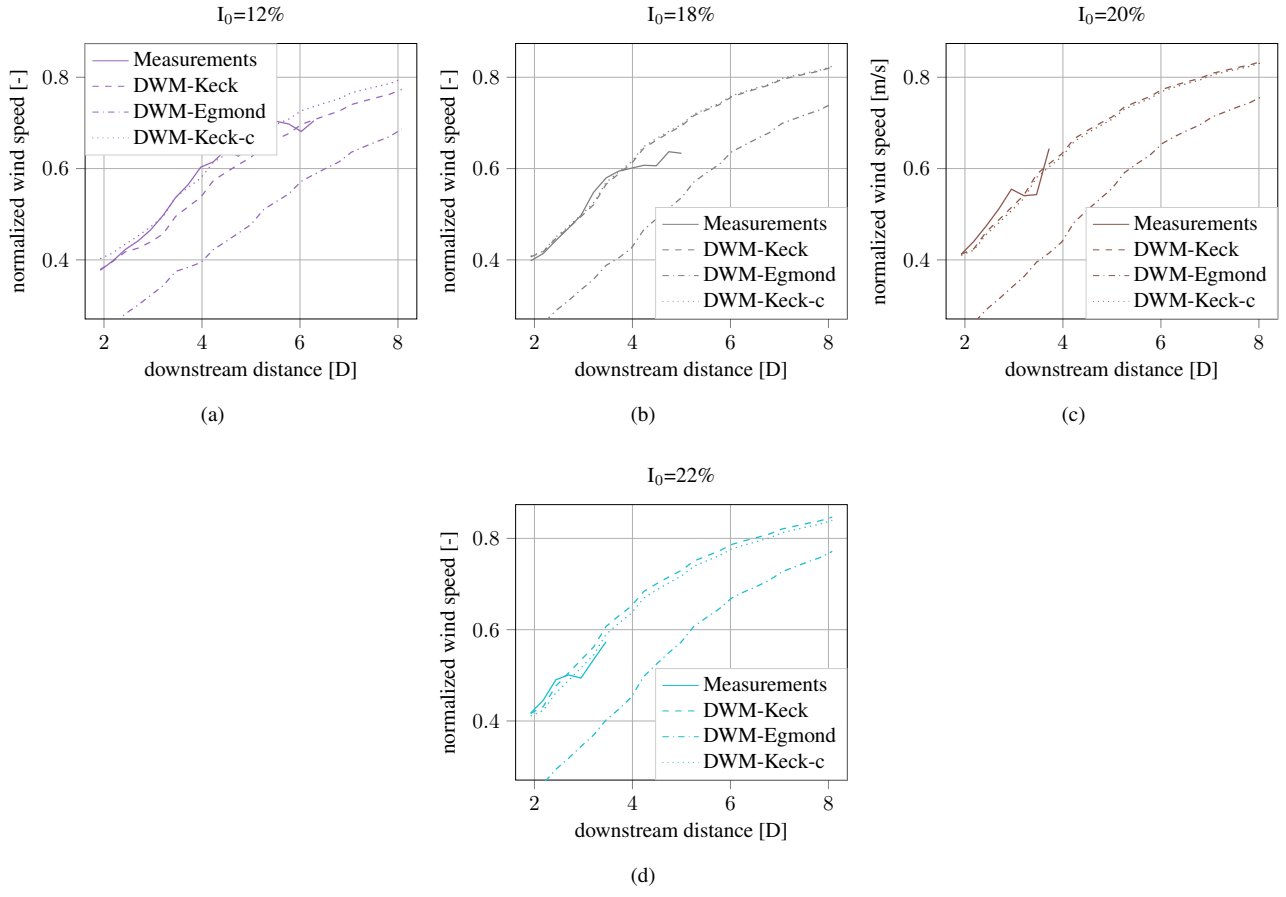

Figure B2. Comparison of measurements and simulations of the minimum wind speed deficit in the MFR for different downstream distances. The recalibrated model is denoted DWM-Keck-c.

References

Ainslie, J. F.: Calculating the flowfield in the wake of wind turbines, J. Wind Eng. Ind. Aerodyn., 27, 213–224, 1988.

Bingöl, F., Mann, J., and Larsen, G. C.: Light detection and ranging measurements of wake dynamics Part I: One-dimensional scanning, Wind Energy, 13, 51–61, https://doi.org/10.1002/we.352, 2010.

Frandsen, S.: Turbulence and turbulence-generated structural loading in wind turbine clusters, Ph.D. thesis, Technical University of Denmark, 2007.

Gerke, N., Reinwardt, I., Dalhoff, P., Dehn, M., and Moser, W.: Validation of turbulence models through SCADA data, JPCS, 1037, 072 027, https://doi.org/10.1088/1742-6596/1037/7/072027, 2018.

IEC 61400-1 Ed.4: IEC 61400-1 Ed. 4: Wind energy generation systems - Part 1: Design requirements, Guideline, International Electrotechnical Commission (IEC), 2019.

https://doi.org/10.5194/wes-2019-89
Preprint. Discussion started: 4 December 2019
© Author(s) 2019. CC BY 4.0 License.

Keck, R.-E.: A consistent turbulence formulation for the dynamic wake meandering model in the atmospheric boundary layer, Ph.D. thesis, Technical University of Denmark, 2013.

Keck, R.-E., de Maré, M., Churchfield, M. J., Lee, S., Larsen, G., and Madsen, H. A.: On atmospheric stability in the dynamic wake meandering model, Wind Energy, 17, 1689–1710, 2014.

Larsen, G. C., Madsen, H. A., Bingöl, F., Mann, J., Ott, S. r., Sørensen, J. N., Okulov, V., Troldborg, N., Nielsen, M., Thomsen, K., Larsen, T. J., and Mikkelsen, R.: Dynamic wake meandering modeling, Tech. Rep. Risø-R-1607(EN), Risø National Laboratory, 2007.

Larsen, G. C., Madsen, H. A., Larsen, T. J., and Troldborg, N.: Wake modeling and simulation, Tech. Rep. Risø-R-1653(EN), Risø National Laboratory for Sustainable Energy, 2008a.

Larsen, G. C., Madsen, H. A., Thomsen, K., and Larsen, T. J.: Wake meandering: A pragmatic approach, Wind Energy, 11, 377–395, https://doi.org/10.1002/we.267, 2008b.

Larsen, T. J., Madsen, H. A., Larsen, G. C., and Hansen, K. S.: Validation of the dynamic wake meander model for loads and power production in the Egmond aan Zee wind farm, Wind Energy, 16, 605–624, 2013.

Machefaux, E., Troldborg, N., Larsen, G., Mann, J., and Aagaard Madsen, H.: Experimental and numerical study of wake to wake interaction in wind farms, in: Proceedings of EWEA 2012 - European Wind Energy Conference & Exhibition, European Wind Energy Association (EWEA), 2012.

Machefaux, E., Larsen, G. C., Troldborg, N., and Rettenmeier, A.: Single wake meandering, advection and expansion - An analysis using an adapted pulsed lidar and CFD LES-ACL simulations, in: Prodeedings of EWEA 2013 - European Wind Energy Conference & Exhibition, European Wind Energy Association (EWEA), 2013.

Machefaux, E., Larsen, G. C., Troldborg, N., Gaunaa, M., and Rettenmeier, A.: Empirical modeling of single-wake advection and expansion using full-scale pulsed lidar-based measurements, Wind Energy, 18, 2085–2103, https://doi.org/10.1002/we.1805, 2015.

Machefaux, E., Larsen, G. C., Troldborg, N., Hansen, K. S., Angelou, N., Mikkelsen, T., and Mann, J.: Investigation of wake interaction using full-scale lidar measurements and large eddy simulation, 19, 1535–1551, https://doi.org/10.1002/we.1936, 2016.

Madsen, H. A., Larsen, G. C., Larsen, T. J., and Troldborg, N.: Calibration and validation of the dynamic wake meandering model for implementation in an aeroelastic code, J. Sol. Energy Eng., 132, 041 014, 2010.

Reinwardt, I., Gerke, N., Dalhoff, P., Steudel, D., and Moser, W.: Validation of wind turbine wake models with focus on the dynamic wake meandering model, JPCS, 1037, 072 028, https://doi.org/10.1088/1742-6596/1037/7/072028, 2018.

Trujillo, J.-J., Bingöl, F., Larsen, G. C., Mann, J., and Kühn, M.: Light detection and ranging measurements of wake dynamics. Part II: Two-dimensional scanning, Wind Energy, 14, 61–75, https://doi.org/10.1002/we.402, 2011.

Veers, P. S.: Three-Dimensional Wind Simulation, Tech. Rep. SAND88-0152(EN), Sandia National Laboratories, 1988.